International Society for Rock Mechanics and Rock Engineering
Norwegian Group for Rock Mechanics

ISRM International Symposium
Eurock 2025 – Expanding the Underground Space
Trondheim, Norway, 16-20 June
ISBN 978-82-8208-079-8

Investigation of anisotropic failure in slate under thermo-hydro-mechanical coupling using the discrete element method

Chih-Shan Lee, Chia-Hsun Peng, Meng-Chia Weng, Hoang-Khanh Le
Department of Civil Engineering, National Yang Ming Chiao Tung University, Hsinchu, Taiwan.
mcweng@nycu.edu.tw

Abstract

Taiwan, rich in geothermal energy predominantly located in slate-dominated regions, faces significant challenges due to the high anisotropy and heterogeneity of slate. These unique characteristics markedly distinguish its properties from those of isotropic rock. This study examines the thermo-hydro-mechanical (THM) behavior of slate from Eastern Taiwan, focusing on its anisotropic failure characteristics. High-temperature triaxial tests were conducted to develop an anisotropic thermal-mechanical coupling failure criterion (ATMFC), which was incorporated into a user-defined model in the discrete element method software 3DEC. The ATMFC was initially validated through thermal triaxial test simulations and subsequently applied to analyze various benchmark scenarios involving THM coupling behavior. The results underscore the significant effects of anisotropy and thermal degradation on stress and strain distributions, offering valuable insights for the design and operation of geothermal systems in anisotropic rock formations.

Keywords

Anisotropic rock, geothermal, THM coupling, Discrete element method.

1 Introduction

Taiwan is located at the intersection of tectonic plates, resulting in intense orogeny and extensive metamorphism, which in turn endows the island with abundant geothermal resources. Unlike many other regions, most of Taiwan's geothermal resources on the eastern side are found within slate, a type of metamorphic rock. The slate in the Hongye area is characterized by pronounced foliation, which leads to anisotropic strength depending on the direction and orientation of stress relative to the foliation. Using core samples approximately 830 meters in length from the Hongye area, several high-temperature triaxial tests were conducted to develop anisotropic thermal-mechanical coupling failure criteria (Lin, 2023). This study applied the ATMFC model within the 3DEC software. After verifying its accuracy, simulations were performed on benchmark problems under various coupling conditions, including thermal-mechanical (TM), hydraulic-mechanical (HM), and thermal-hydraulic-mechanical (THM) coupling, to analyze failure states and stress path development.

2 Method

2.1 Anisotropic Thermal-Mechanical coupling Failure Criteria (ATMFC)

Weng et al. (2024) conducted high-temperature and pressure triaxial tests on slate.

The results showed that the orientation angle within a specific range significantly influenced the strength of the slate, primarily owing to the foliation strength. Beyond this range, intrinsic rock properties led to different failure modes. Elevated temperatures significantly diminished the strength anisotropy of the slate, a phenomenon consistently observed at different temperatures and confining pressures. These findings provided a foundation for the development of an anisotropic thermal-mechanical coupling failure criteria (ATMFC). The failure type can be sliding failure and non-sliding failure. The sliding failure is adapted from Jaeger's criterion (1960). It can be expressed as below:

$$\sigma_1 = \sigma_3 + \frac{2(c_j + \sigma_3 tan\phi_j)}{sin(2\theta)(1 - tan\theta tan\phi_j)} \quad (1)$$

where c_j is cohesion of foliation at 25°C; ϕ_j is friction angle of foliation at 25°C and θ is orientation angle, the angle between major principal stress and foliation plane.

The non-sliding failure is adapted from Ting's and Kuo's criterion (2006). This study considers anisotropic strength in non-sliding failure of anisotropic rock. It can be expressed as below:

$$\sigma_1 = \sigma_3 + \frac{k\sqrt{m\sigma_3\sigma_c + {\sigma_c}^2}}{cos^4\theta + ksin^4\theta + 2nksin^2\theta cos^2\theta} \quad (2)$$

where k is the ratio of unconfined compressive strength at 0° and 90° orientation angle; m is Hoek and Brown criterion (1980) parameters; σ_c is unconfined compressive strength at 0° orientation angle; n is transversal anisotropy parameter and θ is orientation angle.

Considering the thermal degradation, the non-sliding strength in ATMFC can be expressed as below (3) to (5):

$$\sigma_{1(\theta,T)} = \sigma_3 + (\sigma_{1(\theta,25°C)} - \sigma_3)\frac{(\eta - 1)}{\omega \cdot [1 + e^{(T_i - T)\gamma}]} \quad (3)$$

$$\eta = \frac{\sigma_{1(\theta,100°C)}}{\sigma_{1(\theta,25°C)}} \quad (4)$$

$$\omega = \frac{\sigma_{1(\theta,25°C)} - \sigma_{1(\theta,100°C)}}{\sigma_{1(\theta,25°C)} - \sigma_{1(\theta,200°C)}} \quad (5)$$

where T_i is characteristic temperature and γ is the degradation parameter. The criterion firstly needs to fit test results to get unconfined compressive strength at 100°C and 200°C. ATMFC parameters which used in slate in Hongye are shown as Table 1 and the triaxial test results and ATMFC theoretical strength 3D plane is shown in Figure 1.

Table 1 ATMFC parameters of slate in Hongye

Sliding failure		**Non-sliding failure**	
Parameters	**value**	**Parameters**	**value**
$c_{j,\,25°C}$ (MPa)	1.89	k	0.72
		m	11
		n	1.88
		$\sigma_{c,\,25°C}$ (MPa)	63.9

		$\sigma_{c,\ 100°C}$ (MPa)	39.3
		$\sigma_{c,\ 200°C}$ (MPa)	35.0
$\phi_{j,\ 25°C}$ (°)	27.8	T_i (°C)	85
		γ	0.12

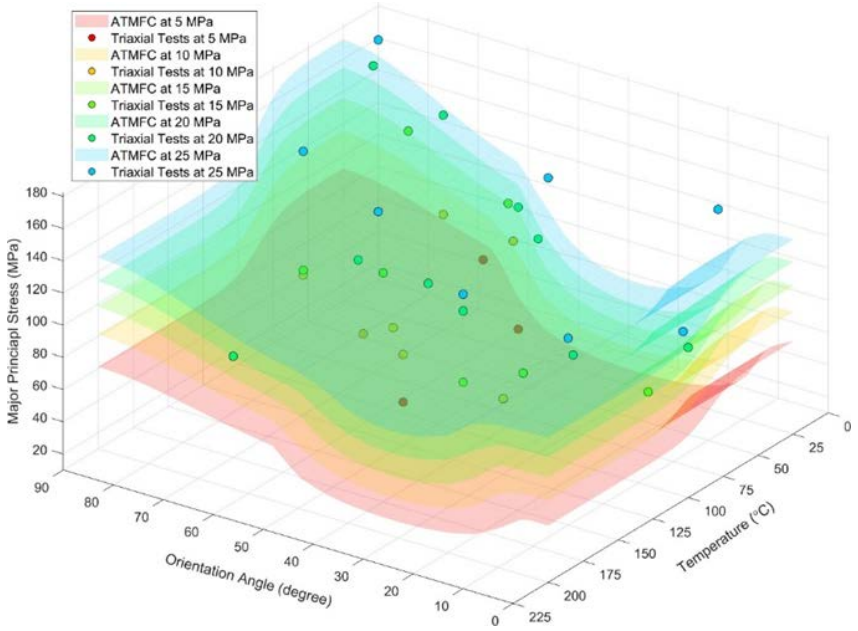

Fig. 1 A three-dimensional illustration depicting the interplay between temperature, orientation angle, and the principal stress at failure, with corresponding test results for slate plotted within the same figure

2.2 Foliation Failure of DEM simulation

The proposed failure criterion was implemented in the 3DEC software using a User-Defined Model (ITASCA, 2020) for analysis. Unlike finite element method software, 3DEC offers the advantage of simulating separation behavior effectively. Two distinct constitutive models, referred to as Cmodel and Jmodel, are used in this study. Table 2 below highlights the differences between these models:

Table 2 Comparison of Cmodel and Jmodel

Items	**Cmodel**	**Jmodel**
Applicable objects	Block (3D)	Discontinuity (2D)
Deformation parameters	Young's modulus, Poisson's ratio	Shear stiffness, Normal Stiffness
Separation or not	No	Split the block and the plane can slip even separate

Based on the triaxial tests on slate conducted by Weng et al. (2024), the model was constructed in a cylindrical shape to simulate two conditions: Cmodel and Cmodel+Jmodel. The Cmodel+Jmodel incorporates foliation into the model, enabling slip and even separation, which leads to a pronounced drop in strength after reaching the peak value (Fig. 2). At a test temperature of 100°C under varying confining stresses, the simulation results align well with the anisotropic thermal-mechanical coupling failure criterion (ATMFC), as shown in Fig. 3.

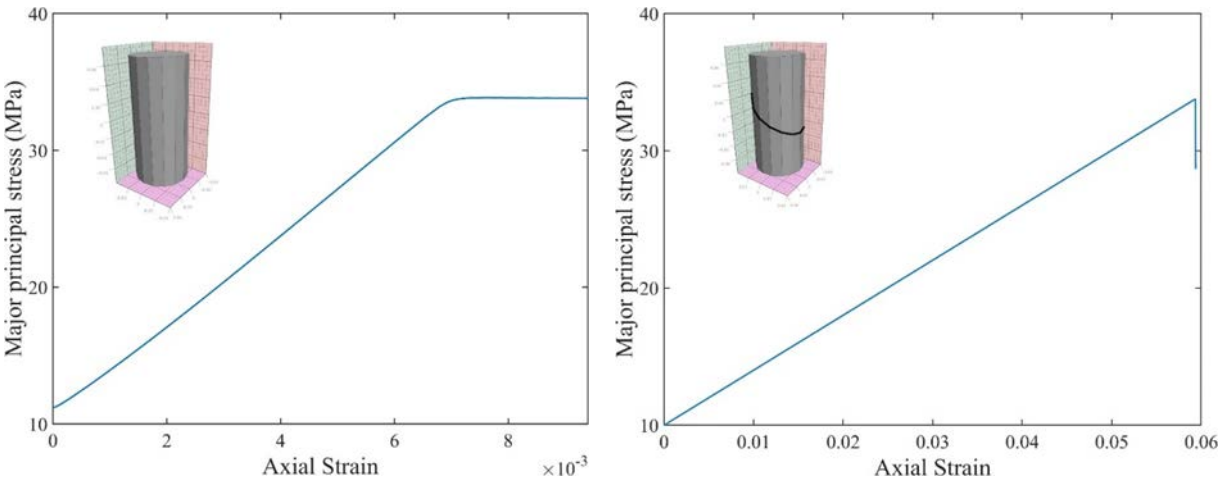

Fig. 2 Stress-strain development in Cmodel (left) and Cmodel+Jmodel (right)

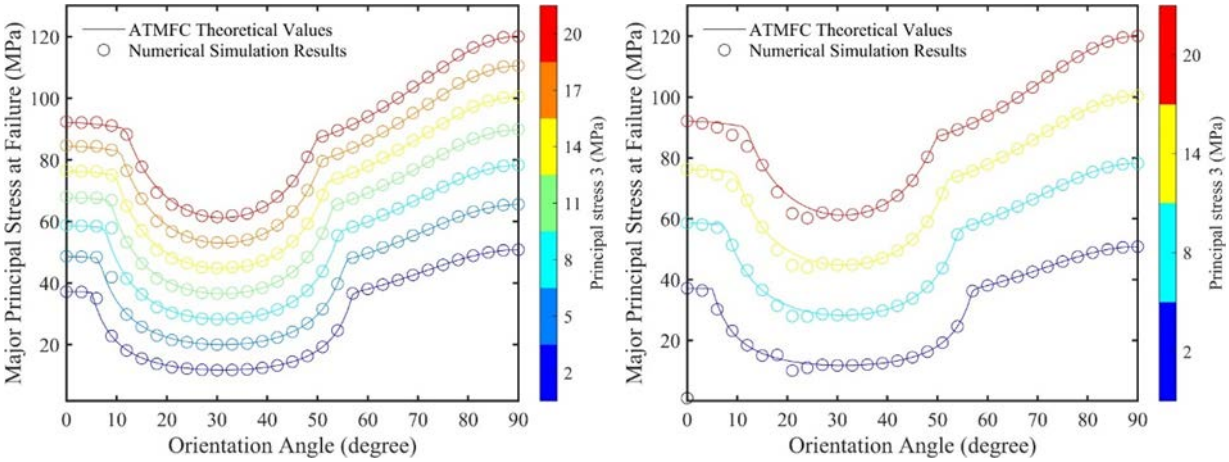

Fig. 3 The comparison of simulation result and ATMFC theoretical values, Cmodel(left) and Cmodel+Jmodel(right)

3 Benchmark Problem

The U.S. Department of Energy (2016) proposed the Benchmark problem of geothermal techniques for different academic fields, which could be used to carry out numerical simulation and analysis related to fracture mechanics and high-pressure fluid injection. The Benchmark problem was introduced as a plane strain condition, in which an isotropic elastic rock contained a 45° fracture in the XY plane. The rock mass was subjected to the maximum and minimum principal stresses of 20 MPa and 13 MPa, respectively. A continuous flow of water was injected into the center of the fracture, resulting in an initial pore pressure of 10 MPa for 180 days. This study also used the benchmark problem to establish the hydraulic-mechanical coupled model in 3DEC considering the influence of hydraulic fracturing behavior on the rock mass under different δ angles (0^o, 45^o, 90^o, and 135^o) (Fig. 4a). δ is the angle intersected by the fracture and the foliation. A complete 3DEC model ($\delta = 0^o$) with dimensions of 160 m×160 m×10 m was illustrated in Fig. 4b. The fracture with a length of 40 m was created in the center of the model. The microparameters for foliation, fracture, and fluid are presented in Tab. 2. Figure 5 shows the failure zone and fracture propagation of rock mass after 180 days of water injection. The result indicated that under different δ, the influence of water injection on the existing fracture of foliated rock was highly different. When $\delta = 0^o$, most damages were observed at two ends of the fracture, the foliation was then opened and damaged severely. The rock mass was slightly damaged along the existing fracture when the foliation was in a vertical direction. When $\delta = 90^o$, the foliation was severely sheared and penetrated the rock mass, while the model with $\delta = 135^o$ indicated the lowest damage without separation of any weak surface. The above result proved that the 3D hydraulic-mechanical coupled model showed a reasonable result and was applicable for conducting further analysis.

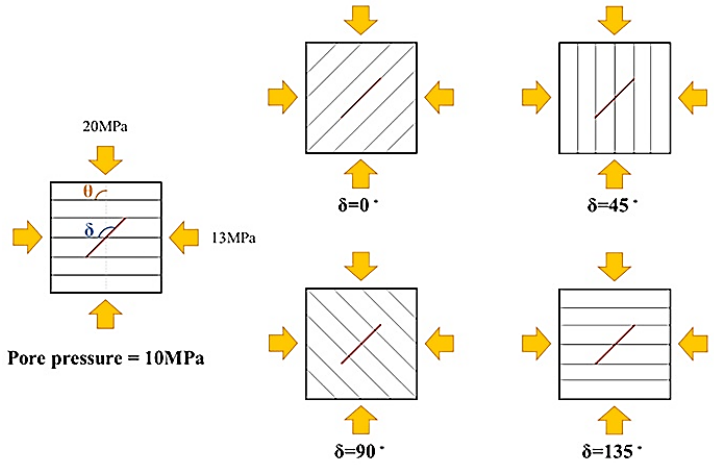

(a) Benchmark problem with different δ

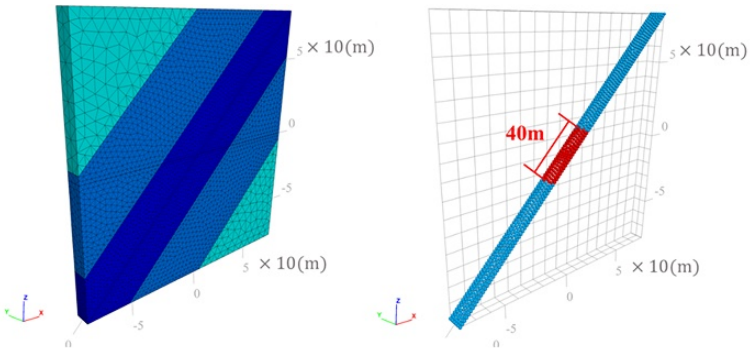

(b) DEM model

Fig. 4. Benchmark three-dimensional hydraulic-mechanical coupled model: (a) The initial conditions of the model and the definition of four different foliation orientation angles δ, which is the angle between the crack (red) and the foliation (gray); (b) Mesh discretization and permeable fracture length of the model in DEM (fluid can flow through the host rock).

Furthermore, simulations were conducted under three distinct coupling conditions: Thermal-Mechanical (TM) coupling, Hydraulic-Mechanical (HM) coupling, and Thermal-Hydraulic-Mechanical (THM) coupling. The benchmark problem was analyzed using two scenarios: the Cmodel condition, which does not include separable foliation, and the Cmodel+Jmodel condition, which incorporates separable foliation with a spacing of 2.5 meters. The inclusion of separable foliation in the Cmodel+Jmodel condition allowed for a more accurate representation of anisotropic failure mechanisms. The parameters used in the benchmark problem are summarized in Table 3.

Table 3 Material parameters of benchmark problem 6 with slate

Parameter	**Units**	**Value**
Elastic Parameters (Rock)		
Young's modulus, *E*	GPa	7.63
Poisson's ratio, ν	--	0.22
Thermal Parameters (Rock)		
Coefficient of thermal expansion, α	μm/m-°C	4.5
Specific heat, *c*	J/g-°C	760
Thermal conductivity, *k*	W/m-K	2.55
Fracture Parameters		
Cohesion, *C*	MPa	0
Friction angle, ϕ	degree	30

Dilation angle, ψ	degree	5
Shear stiffness, k_n	GPa/m	50
Normal stiffness, k_s	GPa/m	3
Fracture aperture initial, b_{ini}	mm	1
Hydraulic aperture	mm	8×10^{-3}
Hydraulic Parameters (Rock)		
Permeability, k_m	m^2	1×10^{-19}
Porosity, ψ_m	%	0.025
Biot's coefficient	--	0.44
Fluid Parameters (Water)		
Density	kg/m3	1000
Fluid bulk modulus, K_f	MPa	275
Specific heat, c	J/g·°C	4200
Thermal conductivity, k	W/m-K	0.5789
Convective Heat-Trans. Coefficient, h	W/m2-K	100
Viscosity, μ	Pa-s	3.547×10^{-4}
Compressibility	M/Pa	4.2×10^{-4}

The results of the foliation failure pattern after 180 days of simulation are presented in Fig. 5. Under the same coupling conditions, foliation with a 90-degree anisotropic angle exhibits the largest failure area. Compared to other anisotropic angles, the initial failure in the foliation predominantly begins at both ends of the injection fracture, highlighting the influence of anisotropy on the failure mechanism.

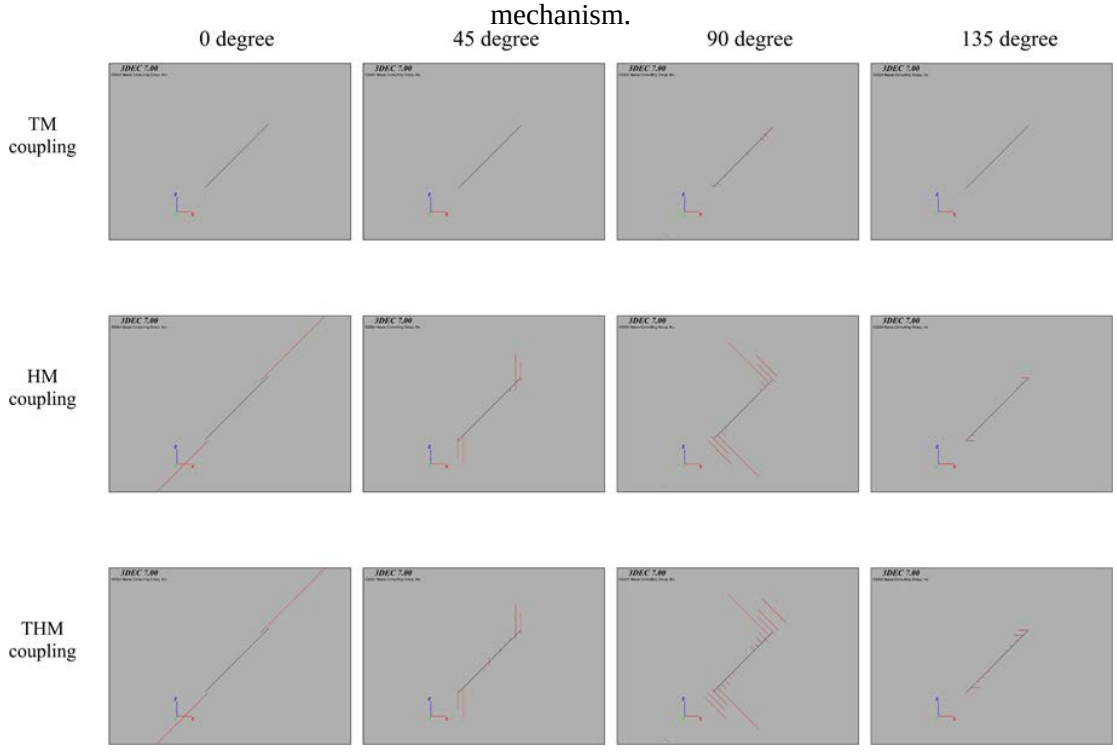

Fig. 5 Results of foliation failure pattern of slate in benchmark problem under 4 different anisotropic angle (X-axis) and 3 different coupling condition (Y-axis)

The development of the failure area over time is illustrated in Fig. 6. For THM coupling, the final failure area ratio for anisotropic angles of 0°, 45°, 90°, and 135° is approximately 4:5:13:2. A similar trend is observed in both HM and THM coupling under the same anisotropic angles, although THM coupling progresses slightly earlier than HM coupling. Notably, except for the 0° anisotropic angle, the rate of failure development slows down over time. This deceleration may result from shear dilation along the failure foliation, which reduces the aperture near the failed foliation. By setting a monitoring point at the upper end of the injection fracture, the stress path of the foliation is analyzed. In TM coupling, the normal stress at the monitoring point continuously decreases. Under HM coupling, the normal stress still decreases, but the shear stress increases. In THM coupling, the stress path initially follows the TM coupling trend, with the normal stress decreasing. As thermal effects dominate in the early stages, the stress path shifts to align with the HM coupling trend. Consequently, foliation under THM coupling is more likely to reach the failure envelope. This behavior is particularly evident for the 90-degree anisotropic angle, as demonstrated in the stress path analysis shown in Fig. 7.

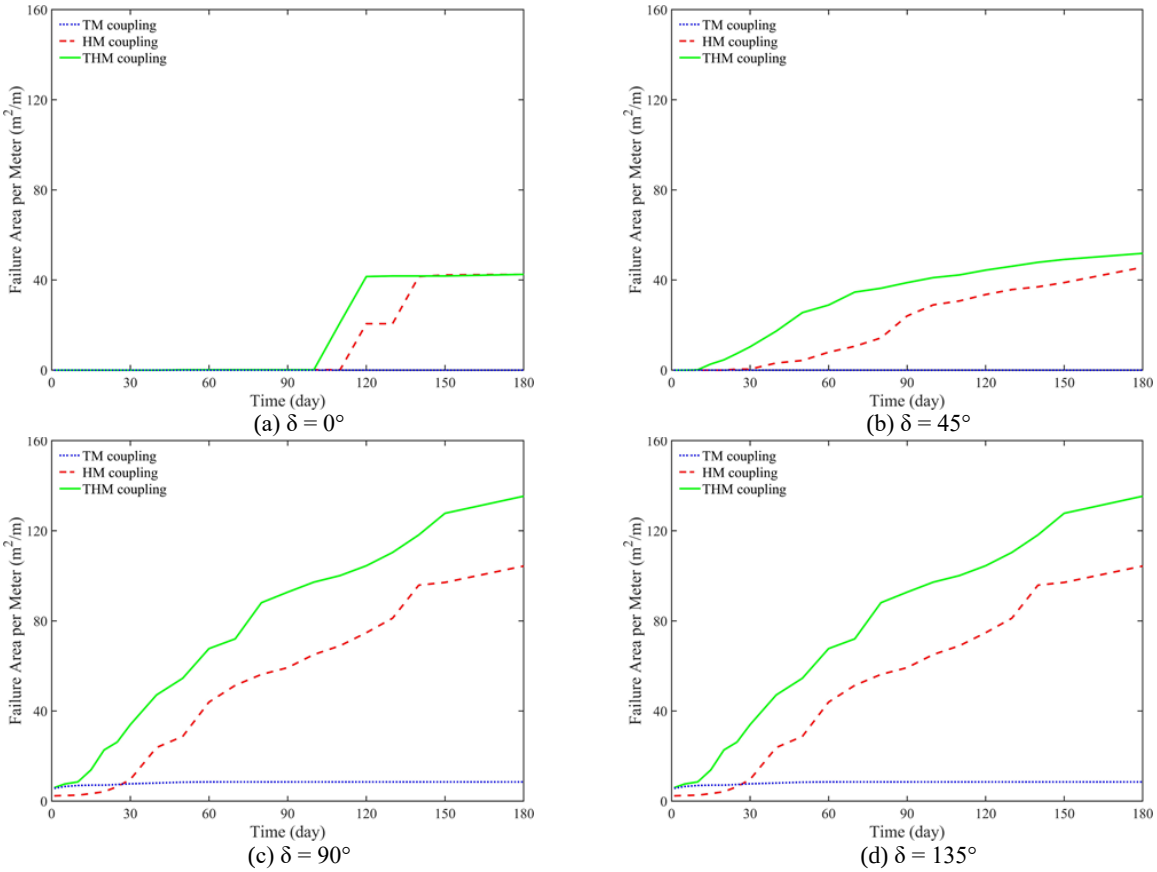

(a) δ = 0° (b) δ = 45°

(c) δ = 90° (d) δ = 135°

Fig. 6 Foliation failure area development under different anisotropic angle

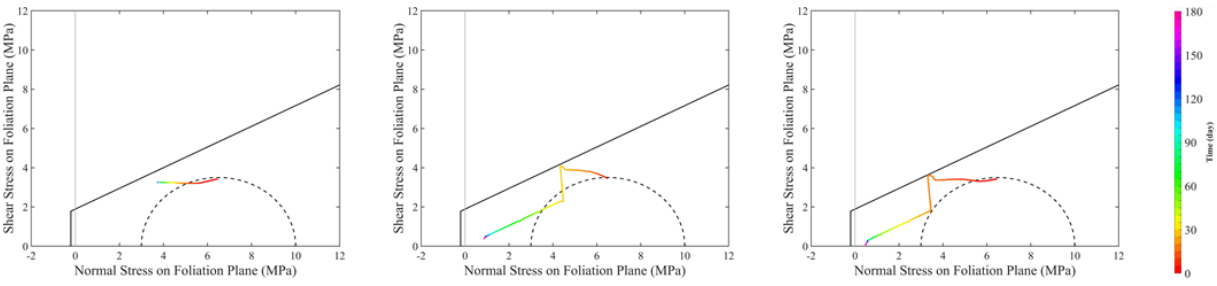

(a) TM coupling (b) HM coupling (c) THM coupling

Fig. 7 Stress path at upper end of injection fracture with 90 degree anisotropic angle

4 Conclusion

This study successfully integrates the anisotropic thermal-mechanical coupling failure criterion (ATMFC) model into the numerical software 3DEC, achieving simulation results for high-temperature triaxial tests that closely align with ATMFC theoretical values. In the benchmark analysis, the

behavior under Thermal-Hydraulic-Mechanical (THM) coupling can be interpreted as a superposition of Thermal-Mechanical (TM) coupling and Hydraulic-Mechanical (HM) coupling. Initially, the response follows the TM coupling trend before transitioning to the HM coupling trend. As the foliation strength remains constant with varying temperatures while volumetric stress decreases with increasing temperature, foliations are more susceptible to failure under THM coupling than under HM coupling. Conversely, matrix strength exhibits an initial decrease followed by an increase due to the influence of ATMFC. These findings provided valuable insights for the evaluation of geothermal development in slate areas and enhanced the understanding of the THM behavior of these materials in geothermal reservoirs.

References

Jaeger JC, Cook NGW (1979) Fundamentals of Rock Mechanics, 3rd Ed. Wiley-Blackwell, New York

Amadei B (1986) Rock Anisotropy and the Theory of Stress Measurements. Springer Verlag, Berlin.

Tien, YM, Kuo MC (2001) A failure criterion for transversely isotropic rocks. International Journal of Rock Mechanics & Mining Sciences 38, 399–412

Asadi M, Bagheripour MH (2015) Modified criteria for sliding and non-sliding failure of anisotropic jointed rocks. International Journal of Rock Mechanics & Mining Sciences, 73, 95-101.

Pacific Northwest National Laboratory (2016) Benchmark Problems of the Geothermal Technologies Office Code Comparison Study. U.S Department of Energy

Itasca Consulting Group, Inc. (2020) 3DEC — Three-Dimensional Distinct Element Code, Ver. 7.0. Minneapolis: Itasca.

Shiu WJ, Weng MC, Chiu CC, Wu PL (2021) Evaluating coupled hydro-mechanical behavior of anisotropic rock mass using DEM. Bulletin of Engineering Geology and the Environment 81, 3.

Wang KX, Liu ZB (2022) Performance of enhanced geothermal system with varying injection-production parameters and reservoir properties. Applied Thermal Engineering, 207, 118160

Weng MC, Li HH, Fu YY, Fang CH, Chen HR, Chang CY (2022) A failure criterion for foliation and its application for strength estimation of foliated metamorphic rock. International Journal of Rock Mechanical & Mining Sciences, 153,105086.

Wu ZJ, Cui WJ, Weng L, Liu QS(2023) Modeling Geothermal Heat Extraction-Induced Potential Fault Activation by Developing an FDEM-Based THM Coupling Scheme. Rock Mechanics and Rock Engineering, 56, 3279-3299

Jack H N, Timothy M L (2023) Commercial-Scale Demonstration of a First-of-a-Kind Enhanced Geothermal System. EarthArXiv

Liu B, Meng W, Zhao ZH (2023) Coupled thermal-hydro-mechanical modeling on characteristics of excavation damage zone around deep tunnels crossing a major fault. Tunnelling and Underground Space Technology, 134 105008

Weng MC, Lin SS, Lee CS, Wu WH, Li JH, Liu CH (2024) An anisotropic thermal-mechanical coupling failure criterion for slate. Rock Mechanics and Rock Engineering, 57, 8157–8177